Study on the transient flow induced by the windbreak transition regions in a railway subject to crosswinds

Chen, Zheng Wei; Hashmi, Syeda Anam; Liu, Tang Hong; Li, Wen Hui; Sun, Zhuang; Liu, Dong Run; Hemida, Hassan; Liu, Hong Kang

DOI:
10.12989/was.2022.35.5.309

Document Version
Peer reviewed version

Citation for published version (Harvard):
Chen, ZW, Hashmi, SA, Liu, TH, Li, WH, Sun, Z, Liu, DR, Hemida, H & Liu, HK 2022, 'Study on the transient flow induced by the windbreak transition regions in a railway subject to crosswinds', *Wind and Structures, An International Journal*, vol. 35, no. 5, pp. 309-322. https://doi.org/10.12989/was.2022.35.5.309

Study on the transient flow induced by the windbreak transition regions in a railway subject to crosswinds

Zheng-Wei Chen[1a], Syeda Anam Hashmi[3b], Tang-Hong Liu[2c], Wen-Hui Li[*2], Zhuang Sun[4d], Dong-Run Liu[2e], Hassan Hemida[3f], Hong-Kang Liu[*2]

[1]*Department of Civil and Environmental Engineering, The Hong Kong Polytechnic University, Hung Hom, Kowloon, Hong Kong, PR China*
[2]*Key Laboratory of Traffic Safety on Track of Ministry of Education, School of Traffic & Transportation Engineering, Central South University, Changsha 410075, PR China*
[3]*Birmingham Centre for Railway Research and Education, School of Civil Engineering, University of Birmingham B15 2TT, UK*
[4]*Chengdu Fluid Dynamics Innovation Center, Chengdu 610072, PR China*

(Received keep as blank , Revised keep as blank , Accepted keep as blank)

Abstract. Due to the complex terrain around high-speed railways, the windbreaks were established along different landforms, resulting in irregular windbreak transition regions between different subgrade infrastructures (flat ground, cutting, embankment, etc). In this paper, the effect of a windbreak transition on the wind flow around railways subjected to crosswinds was studied. Wind tunnel testing was conducted to study the wind speed change around a windbreak transition on flat ground with a uniform wind speed inflow, and the collected data were used to validate a numerical simulation based on a detached eddy simulation method. The validated numerical method was then used to investigate the effect of the windbreak transition from the flat ground to cutting (the "cutting" is a railway subgrade type formed by digging down from the original ground) for three different wind incidence angles of 90°, 75°, and 105°. The deterioration mechanism of the flow fields and the reasons behind the occurrence of the peak wind velocities were explained in detail. The results showed that for the windbreak transition on flat ground, the impact was small. For the transition from the flat ground to the cutting, the influence was relatively large. The significant increase in the wind speeds was due to the right-angle structure of the windbreak transition, which resulted in sudden changes of the wind velocity as well as the direction. In addition, the height mismatch in the transition region worsened the protective effect of a typical windbreak.

Keywords: railway; crosswinds; windbreak transition; flow structures; wind tunnel test; computational fluid dynamics (CFD)

1. Introduction

The effects of strong crosswinds on railways are global problems, and accidents involving the overturning of trains, and the vibration of pantograph-catenary systems, due to the impact of strong winds are often reported (Diedrichs *et al.* 2007; Baker *et al.* 2009; Gao *et al.* 2021; Dong *et al.* 2022; Liu *et al.* 2022). As a result, the aerodynamic performances of trains experiencing crosswinds have been investigated extensively in previous research (Hemida and Krajnović 2008; Tsubokura *et al.* 2010; Chen *et al.* 2018; Tunay *et al.* 2018; Chen *et al.* 2019; Hashmi *et al.* 2019; Gu *et al.* 2020; Guo *et al.* 2020; Huo *et al.* 2021; Li *et al.* 2022). In addition, the dynamic safety of trains experiencing crosswinds has become a popular topic of investigation using different methods, such as the three-mass model or multi-body system dynamics. These methods have been used to obtain the critical wind curves for setting up a safe operating range for trains exposed to crosswinds (Cheli *et al.* 2010; Cui *et al.* 2014; Liu *et al.* 2018). However, most of the previous studies have only discussed a constant wind speed. In reality, trains are usually subjected to unsteady winds. The speeds and directions of the wind along the railway lines are not uniform, and are subjected to large variations because railway lines pass from either viaducts, tunnels, cuttings, or embankments. Thus, the wind velocity is expected to change suddenly in the connection positions of different terrains (Yu *et al.* 2019). Zhang *et al.* (2019) studied the aerodynamics of a scaled train model in the transition region between the subgrade (including the cutting and embankment) and tunnel during crosswinds. The results showed that the impact of the transition from the cutting to the tunnel was larger than that of the embankment–tunnel transition. The effects of long-span bridge towers on trains were investigated by Li *et al.* (2013) using wind tunnel tests. The results of their study demonstrated that due to the shielding effects of the towers, the aerodynamic performances of the trains were considerably affected by the sudden change of the wind load.

*Corresponding author, Ph.D., E-mail: lwh@csu.edu.cn; liuhongkang@csu.edu.cn
[a] Ph.D., E-mail: zhengwei.chen@polyu.edu.hk
[b] Ph.D., E-mail: sah232@bham.ac.uk
[c] Professor, E-mail: lth@csu.edu.cn
[d] Ph.D., E-mail: sunzhuang802@163.com
[e] Ph.D., E-mail: csuldr@foxmail.com
[f] Reader, E-mail: h.hemida@bham.ac.uk

The results also indicated dramatic fluctuations of the corresponding dynamic responses. Such fluctuations had negative effects on the running safety and passenger comfort of the train. Krajnovic (2008) investigated the flow structures around an ICE2 train exiting a tunnel under the influence of a wind gust using detached eddy simulation. The results showed that the maximal yawing and rolling moments that could possibly cause derailment and the overturning of trains were likely to occur when one-third or half of the whole train had run out of the tunnel. Furthermore, Krajnović *et al.* (2012) studied the aerodynamics of a simplified train through the wind tunnel test. They compared the aerodynamic test results for a stationary model and a moving model, and it was found that the several aerodynamic coefficients of the moving case were more significant than those of the stationary case.

In strong wind areas, protective measures are always employed to reduce the influence of crosswinds on trains. To do so, different methods exist, such as optimising the train shape, establishing wind forecasting and warning systems, and installing windproof facilities (Tian 2010; Tian 2019; Niu *et al.* 2022). In addition, Chen *et al.* (2022) studied a novel blowing measure to reduce the effect of crosswinds, and they also compared different mitigation effects of different blowing positions on the train surface. In particular, windbreaks are often used in windy areas due to their economic advantages, effectiveness, and reliability, including civil engineering and agricultural engineering (Boldes *et al.* 2001; Boldes *et al.* 2002; Mohebbi and Rezvani 2018; Mohebbi and Rezvani 2019; Pieris *et al.* 2020; Mohebbi and Rezvani 2021; Mohebbi and Safaee 2021). Therefore, the aerodynamic performances and safety of trains exposed to crosswinds with regard to different windbreak structures have been studied by many researchers (Niu *et al.* 2018; Hashmi *et al.* 2019; He *et al.* 2019). It must be noted that in reality, complex kinds of terrain surround these types of windbreak structures (Chen and Ni 2022). Therefore, it is highly likely that such terrain will result in transition regions between the different types of windbreaks. These geometric discontinuities in the windbreak structures cause sudden changes in the flow fields around the railway lines. Some researchers have investigated this problem. For windbreak and open-cut tunnel facilities, Yang *et al.* (2019) and Deng *et al.* (2019) compared the aerodynamic loads and corresponding dynamic safety of windproof facilities when high-speed trains passed through them. Moreover, the transition from a viaduct to a cutting during crosswinds leads to changes in the structural form of the railway. Li *et al.* (2019) investigated the effects of this structure transition based on a 1:20 wind tunnel test. For a windbreak placed along a railway line, a windbreak breach sometimes occurs due to construction issues or accidents. Sun *et al.* (2021) studied the dynamic performance of a high-speed train passing through a windbreak breach during unsteady crosswinds.

In addition to the above, the Lanzhou-Xinjiang passenger railway in China passed through an area with strong winds (Liu *et al.* 2018). A windbreak wall was built along the railway line, but part of the wall passed through mountainous terrain. This resulted in several ground scenarios including flat ground, embankments, and cuttings. Therefore, the windbreaks were discontinuous, which resulted in many transition regions between the flat ground/embankment and cuttings, as shown in Fig. 1. Full-scale tests were conducted and it was shown that when trains passed through transition regions in the windbreaks, a yawing phenomenon occurred. The aerodynamic performances and dynamic indexes of the vehicle system showed sudden changes and became worse, mainly in the position of the discontinuous transition region (Liu *et al.* 2018; Xu *et al.* 2019; Liu *et al.* 2022). This had an effect on both the passenger comfort and the operational safety. Focusing on this issue, Liu *et al.* (2018) and Chen *et al.* (2019) considered real terrain and used a CFD method as well as different dynamic methods to investigate the aerodynamic performance and the dynamic response when a train passed through these transition regions with crosswinds. The studies showed that when the vehicle passed the rectangular transition region, the dynamic parameters strongly varied with the aerodynamic forces, while after the excitation, the dynamic parameters required a longer time to return to a stable state.

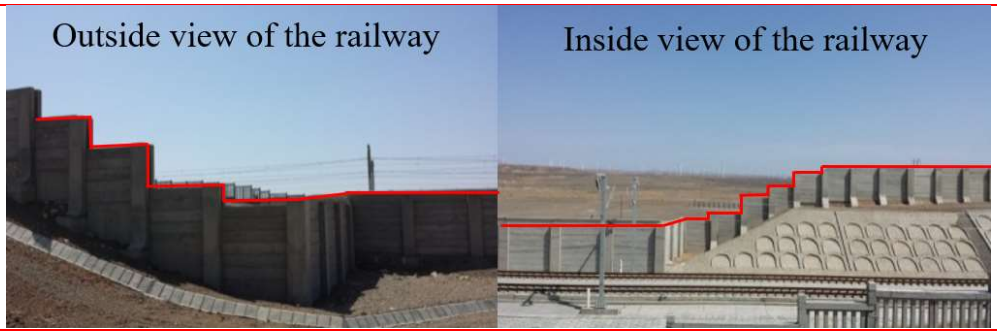

Fig. 1 Windbreak transition region along the railway

It is worth mentioning that while previous works showed various insights into the transition region issue, these studies were mainly focused on the train body, whereas in reality, it is important to understand the wind velocity and flow field changes induced by a windbreak transition to avoid consequences. Equally important, the flow field deterioration mechanism around the windbreak transition regions needs to be understood. Earlier works have only analysed the corresponding effects on the train bodies while ignoring the procedure and cause of the flow field deterioration around a transition region without a train. Therefore, for the first time, this work aimed to study the changes in flow fields induced

by the transition regions in windbreak structures. This work was intended to discuss the reasoning behind the sudden changes of wind and flow fields around transition regions. Furthermore, this assessment was made for three different wind incidence angles based on the wind attacks experienced by the Lanzhou-Xinjiang railway lines.

The rest of this paper is organized as follows. Section 2 describes the windbreak transition in flat ground with wind tunnel tests and numerical simulation. Furthermore, with consideration of the actual situation, Section 3 discusses in detail the results of the flow field changes induced by the windbreak transition between the flat ground and cutting, which is closer to the real situation. The main conclusions of this work are summarized in Section 4 along with recommendations for future works.

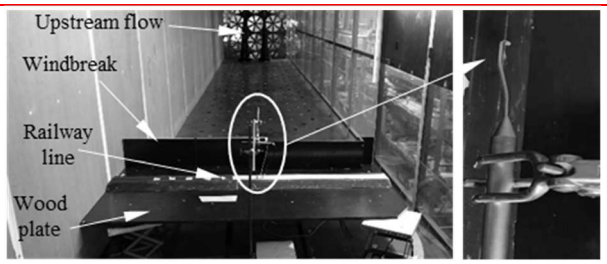

(a) Set-up

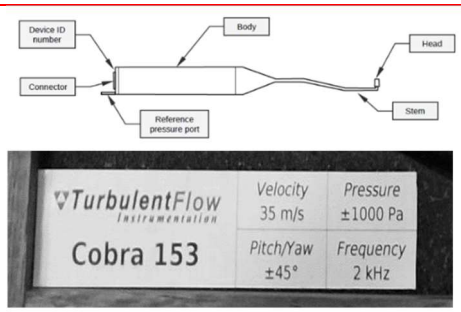

(b) Labelled diagram of Cobra probe

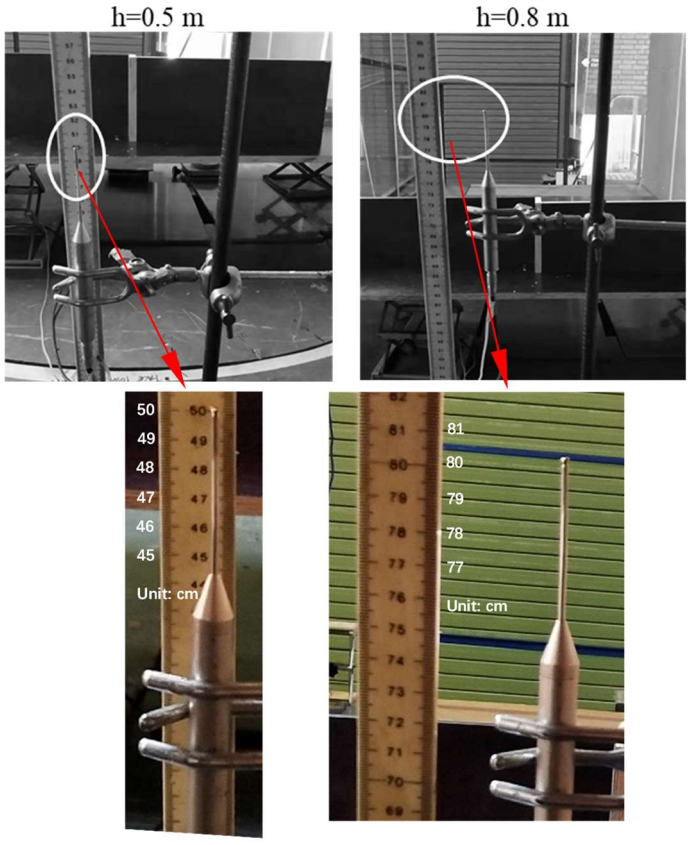

(c) Test position of the upstream flow

Fig. 2 Test models

2. Methodology

In this work, the wind tunnel test and numerical simulation method are comprehensively applied. According to two research objects in this work, namely, windbreak transition on the flat ground and different terrains, the detailed test method and experimental model are introduced in Section 3.1 and the numerical method is introduced in Section 3.2.

3. Windbreak transition on the flat ground

Firstly, to understand the flow structures of the

windbreak transition region along the railway in a simplified scenario, and to verify the numerical method of the following studies, the wind tunnel test was conducted for the case consisting of a windbreak with a transition region in a flat ground scenario.

3.1 Wind tunnel test of windbreak transition on the flat ground

The test was conducted in the University of Birmingham's wind tunnel, which is an open-circuit facility. The width and the height of the wind tunnel were both 2 m. The length of the wind tunnel was 14 m. Once secured, the centre position of the model was 10 m from the upstream inlet. The maximum freestream wind speed was approximately 10 m/s inside the wind tunnel (Hashmi *et al.* 2019). Because the height range of the windbreak in practice was not very high and the wind speed in this height range changed slightly, the ground roughness was not considered in the wind tunnel test. The test model is shown in Fig. 2(a), along with a windbreak, a railway line, and a wooden plate as the ground scenario. To reduce the viscous effects of the ground, the model was installed at a height of 0.3 m above the floor of the wind tunnel. This height was the same as that of Hashmi *et al.* (2019), the same wind tunnel test was conducted with a train model in the reference, it indicated that this height can reflect a real situation, and the detailed boundary layer distribution could be seen in the reference. In addition, as shown in Fig. 2(b), the wind velocity was measured by a Cobra probe with a frequency of 2 kHz (TFI 2015). The test point of the upstream flow was 1.5 m away from the front edge of the wooden plate, as shown in Fig. 2(c). The upstream flow was measured at two heights, 0.5 m (top of the windbreak) and 0.8 m from the floor of the wind tunnel. In this height range, the turbulence intensity was about 5% in the wind tunnel. The wind velocity of the upstream flow was obtained by averaging the wind velocity of these two heights, and the wind incidence angle was maintained at 90°. The models were at a scale of 1:25. The details are provided in Fig. 3. Above the centre of the tracks, the wind velocity was measured along horizontal lines at two heights: h1 = 0.252 m and h2 = 0.292 m. To conduct the measurements, 13 test points along the tracks were monitored at each height. To reduce the random error, the wind velocity at every test point was tested three times and the average value of the three tests was taken.

Dimensionless parameters were used to analyse the wind velocity. The wind velocity was expressed by a dimensionless coefficient, u:

$$u = V/U \quad (1)$$

In the expression, V is the local total wind velocity above the tracks and U is the total upstream flow velocity. Fig. 4 shows the distribution of the wind velocity above the tracks. An obvious change in wind velocity around the right-angle region of a windbreak occurred. The amplitudes of the peak-peak values in the right-angle region at h1 and h2 were 0.68 and 0.39, respectively. As a reference, the test points at y/H = -3.4 and y/H = 3 (the coordinate system refers to Fig. 3; H is the height of the train from the top of the rail, which was 3.7 m in the full-scale) were chosen as the basic values at both sides of the right-angle region. It could be observed that at a height h1 (z/H = 1.70), the ratio between the test point y/H = -0.7 and y/H = -3.4 was 2.63, and the ratio between the test point y/H = -0.7 and y/H = 3 was 1.62. At the height h2 (z/H = 1.97), the corresponding ratios were 1.49 and 1.14. Overall, at a lower height near the top of the windbreak, the effect of the right-angle region was larger, and this right-angle region resulted in rapid changes in the wind velocity from a higher value to an exceedingly small value. However, after a certain distance, the wind velocity tended to become stable again.

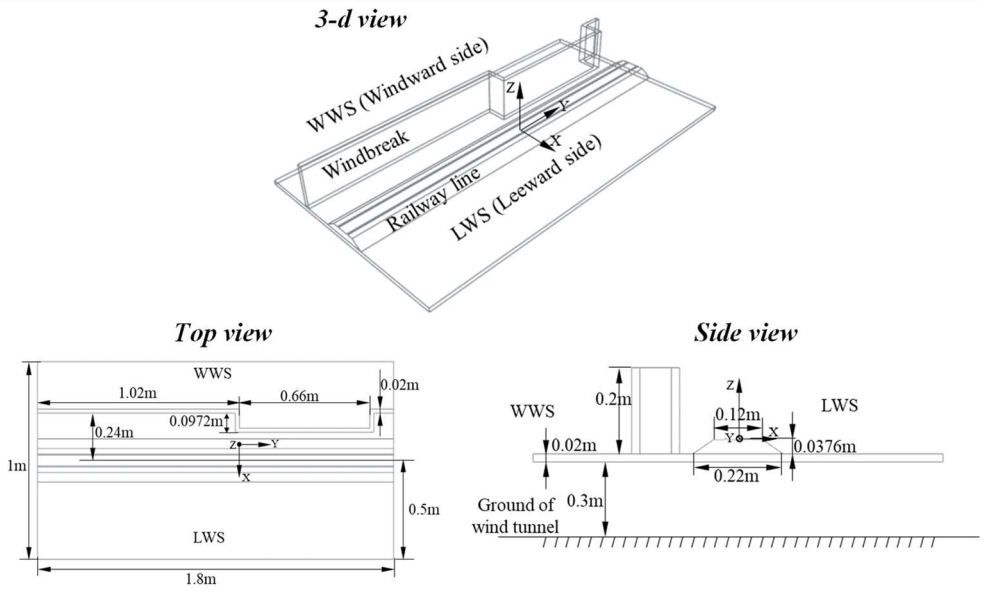

(a) The dimensions

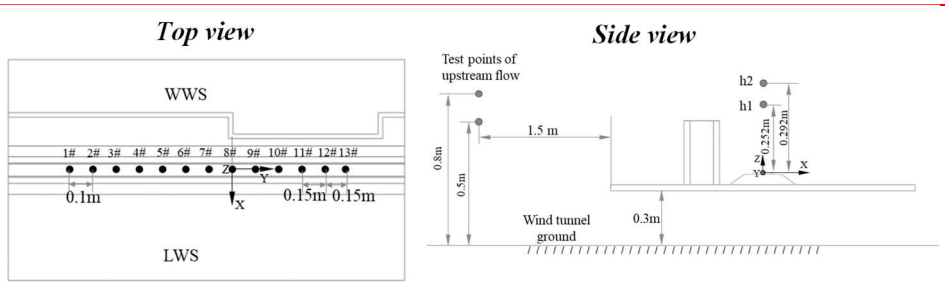

(b) The layout of the test points

Fig. 3 Details of the models

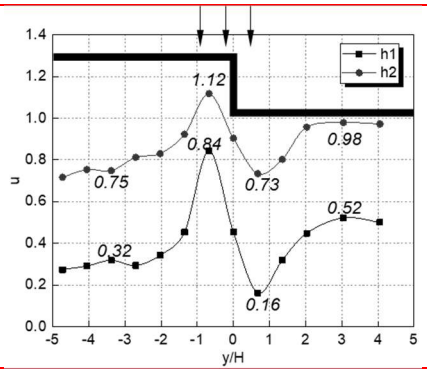

Fig. 4 The test results above the railway line at z/H = 1.70 (h1) and 1.97 (h2)

3.2 Numerical analysis of the wind tunnel test

3.2.1 The numerical method and computational domain

The improved delayed-detached eddy simulation (IDDES) based on the turbulence model SST $k-\omega$ was used in this study. This hybrid numerical method was developed by Shur *et al.* (2008) and it was based on the Reynolds-Averaged Navier-Stokes (RANS) and large eddy simulation (LES) approaches. This method has been used in previous studies and it has demonstrated reliable performance in terms of experimental validation and the flow structure analysis (Flynn *et al.* 2014; Wang *et al.* 2019; Guo *et al.* 2020; Niu *et al.* 2020; Tan *et al.* 2020; Sui *et al.* 2021). It is well known that the traditional DES method will generate modelled-stress depletion (MSD) and grid-induced separation. To solve this problem, a new subgrid length-scale is defined in the delayed detached eddy simulation (DDES) approach developed by Spalart *et al.* (2006). Furthermore, in the present IDDES method, Wall-Model LES (WMLES) is used based on DDES and WMLES used to reduce the limitation of the Reynolds number in near-wall regions. Therefore, the IDDES includes two branches, DDES and WMLES models, as well as a set of empirical functions in order to obtain good performance from these branches and their couplings.

In this study, the governing equations were solved using the finite volume method (FVM) with the solver FLUENT. The pressure-velocity coupling scheme was the Semi-Implicit Method for Pressure Linked Equations-Consistent (SIMPLEC) algorithm developed by Van Doormaal and Raithby (1984). The convection fluxes in the momentum equations were discretized using bounded central differencing, and the turbulent kinetic energy and the turbulent dissipation rate used the second-order upwind scheme. The time integration was conducted using a second order backward implicit scheme, the time steps were maintained at $\Delta t = 1 \times 10^{-4}$ s and the maximum number of iterations was set as 50 for each time step. The Courant-Friedrichs-Lewy (CFL) numbers around the model were less than 1 in more than 90% of the computational cells during the entire simulations. All cases were initially run for 4 seconds to obtain a fully developed flow field equivalent to the flow passing the model more than 30 times, which was then used to average the flow field using data sampling for time-dependent statistics.

The computational model and the domain are shown in Fig. 5. The setups of the computational model were similar to those of the wind tunnel test, including the wind speed and the turbulence intensity. The distance between the windward side (WWS) of the windbreak and face ABCD was 15 H, and 30 H from the leeward side (LWS) of the windbreak to the face EFGH. Corresponding to the wind tunnel test, the face ABCD was set as the velocity inlet, and the face EFGH was set as the zero-pressure outlet, while the other faces were all no-slip wall boundary conditions.

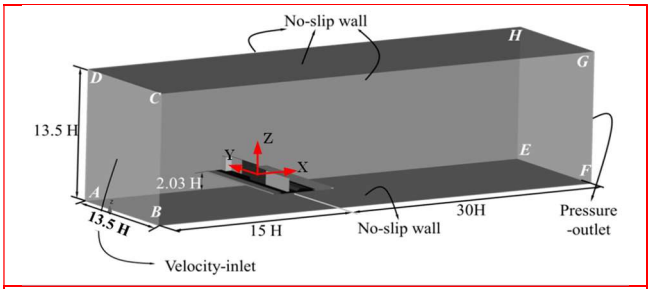

Fig. 5 The computation domain and the boundary conditions

3.2.2 Mesh strategy and experimental validation

Fig. 6(a)–(c) show the three-dimensional (3D) view, side view, and top view of the mesh, respectively. Fig. 6(d) is the surface mesh of the subgrade, and Fig. 6(e)–(f) are the enlarged views of the windbreak mesh. The computational meshes in this work were unstructured hexahedral grids generated using SnappyHexMesh in OpenFOAM. The mesh quality near the object was extra-fine, followed by fine mesh and coarse mesh. To capture the LWS flow field information

accurately, the area of fine and extra-fine mesh in the LWS was set wider than that of the WWS, and there were 10 prism layers around the model. The minimum size around the model was 0.07 mm and the y^+ of the model surfaces was 1–2. Additionally, to determine mesh independence on the simulation results, three meshes including coarse, medium, and fine mesh with corresponding mesh numbers of 10 million, 21 million, and 46 million were tested in this work, as shown in Fig. 7. In the along-wind direction, the velocity component u_x of different meshes at z/H = 0.81 along the centre are shown in Fig. 8(a), and the error between the coarse mesh and the other meshes can be observed. The difference between the medium mesh and the fine mesh was exceedingly smaller than 3%, so a further finer grid was not necessary. Based on the medium mesh, the mesh strategy was compatible with this study, and the results were compared with the lab test results, as shown in Fig. 8(b). In the areas of focus, y/H = -3 ~ 3, it was found that the simulation results had a good agreement with that of the wind tunnel test, and the numerical simulation captured the peak value of the wind velocity accurately in the right-angle transition region. But at a lower position (h1) and far away from the right-angle transition region, there is a relatively larger error because of the better protection effect and smaller wind speed value, such as the position at y/H = -3.4.

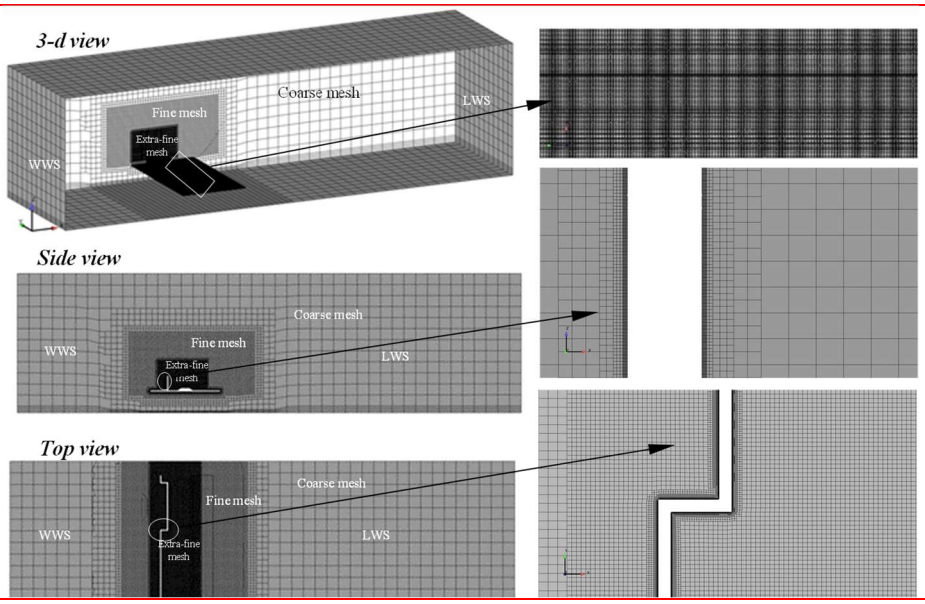

Fig. 6 The computational mesh

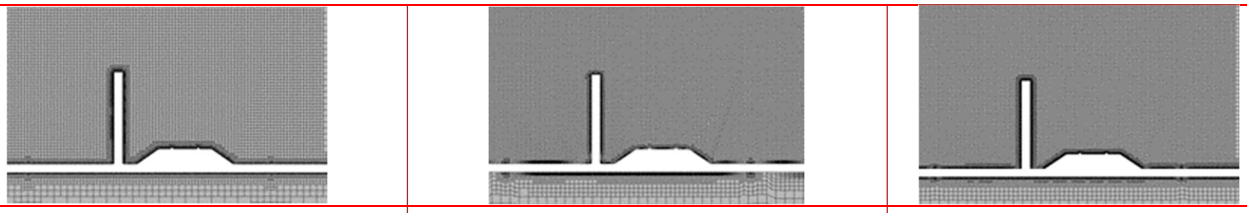

(a) Coarse mesh | (b) Medium mesh | (c) Fine mesh

Fig. 7 The different mesh numbers

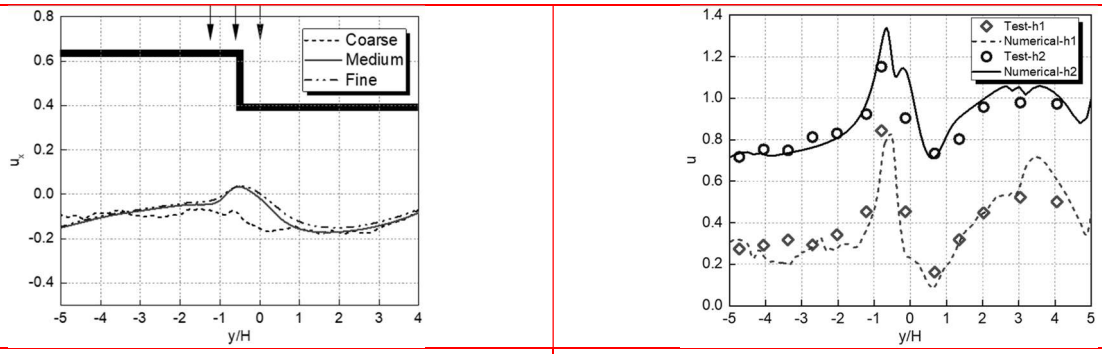

(a) Mesh sensitivity | (b) Comparison between experiment and simulation

Fig. 8 Numerical validation

3.2.3 Flow structures of windbreak transition in the flat ground

Fig. 9 shows the corresponding dimensionless wind speed u along the railway centre, and the wind velocity in each line along the height direction, as well as the position information of y1–y11, can be seen in Fig. 3(c). Overall, in the flat ground, the transition of the windbreak affected the wind velocity slightly below z/H = 1. It can be seen that the wind velocity at most positions was negative due to the better shielding effect of the windbreak, but positive values in the upper position above z/H = 1 occurred for y2–y5. These positive values were highly influenced by the transition of the windbreak, and they resulted in a higher positive wind velocity.

It should be pointed out that the real flow was unsteady, and that the size and locations of the vortexes changed with time. Therefore, the time-average results were used in this work to create a clear and steady description. Fig. 10 shows the time-average streamline at z/H = 0.6 and z/H = 1. Outside the windbreak, vortex V1 was generated in the right-angle transition region. Inside the windbreak, vortexes V2 and V3 were generated on both sides of the right-angle region. In a lower position, z/H = 0.6, the structure sizes of V2 and V3 were exceedingly small and had little effect on the flow field in the railway. However, in a higher position, z/H = 1, the size of V2 and V3 became larger. This generated a strong wind velocity area, as shown in Fig. 10(b), resulting in large positive wind velocity at positions y2–y5 (see in Fig. 9). Additionally, as shown in Fig. 11, from y/H = -2 to y/H = 2, in the LWS, vortexes V4 and V5 were generated by the windbreak, and V6 was generated by the wood edge. V6 would not occur in the real railway. Due to the decreasing distance between the windbreak to subgrade from y/H = -2 to y/H = 2, the development space of V4 was small, resulting in a smaller size V4 between y/H= -2 to y/H= 2. This also caused the vortex core of V5 to move further away from the railway. Comparing locations between y/H= -2 and y/H= 2, it could be seen that the airflow at the top of the windbreak had a downward movement trend at y/H = -0.7, close to the right-angle transition region. This indicated that this region changed the direction and the magnitude of the airflow and decreased the protection effect of the windbreak.

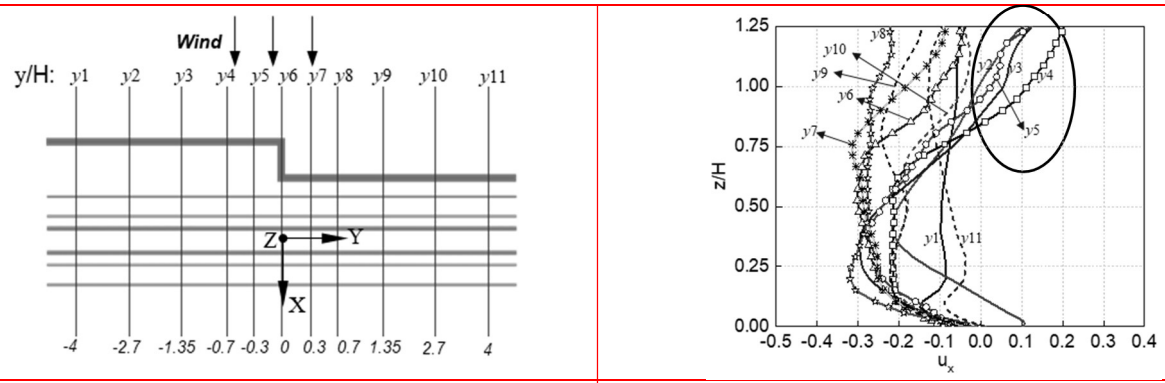

(a) The point positions (b) Wind velocity of y1–y11

Fig. 9 Wind velocity distribution along the railway from y1 to y11

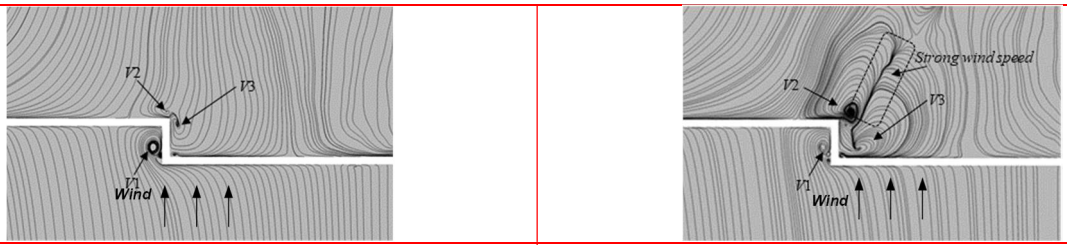

(a) z/H = 0.6 (b) z/H = 1

Fig. 10 The time-average streamline

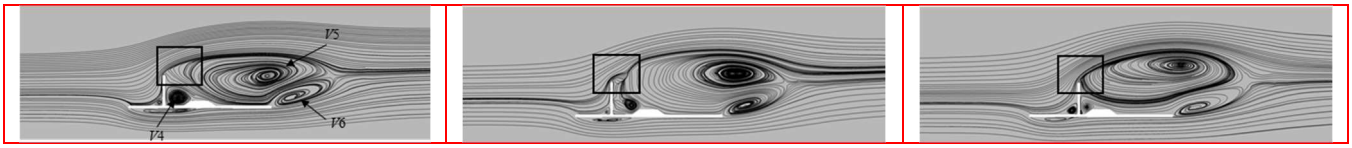

(a) y/H = -2	(b) y/H = -0.7	(c) y/H = 2
Fig. 11 The time-average streamline		

As illustrated in Fig. 12, the velocity contour in the centre of the railway showed that the sudden peak value was not more than 0.35 in the transition region below the height z/H= 1.35, and it was not larger than 0.2 below the height z/H= 1. Therefore, for the case of flat ground outside the windbreak, the right-angle transition region had little effect on the wind field. Finally, note that the current model studied by the wind tunnel test had a short length in the downwind part, so an extra vortex V6 occurred in Fig. 11. In a real situation, it can be sure that the V6 will be disappeared. However, for the wind speed along the center of the railway, the effect of V6 was slight. Therefore, the results in the flat ground were acceptable and could be a reference for the real situation.

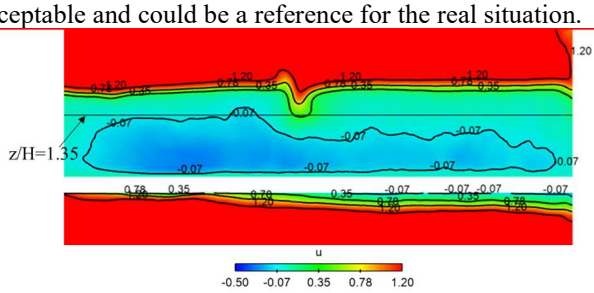

Fig. 12 Velocity contours at the centre of the railway

4. Windbreak transition with terrains

4.1 Model description

To simulate a case that was closer to the practice in Fig. 1, Fig. 13 shows the models of the windbreak transition from the flat ground to the cutting. It should be noted that the shape of transitions on the railway is variable, and a characteristic model was analysed to study the general flow mechanism of this type of transition region in this paper. The flat ground and cutting had lengths of 200 m, and the windbreak transition region had a length of 15 m and a width of 10 m. The windward side (WWS) boundary was 60 m from the centre of double railway lines, and the leeward side (LWS) boundary was 80 m from the same position. Fig. 13(b) shows the detailed sizes of the railway lines, which consisted of two railway lines. Railway line-1 (RL-1) was close to the windbreak and railway line 2 (RL-2) was far from the windbreak wall. The lateral distance between the two lines was 5 m, and the centre of RL-1 was 5.7 m from the windbreak. The windbreak had a height of 4 m and a width of 0.2 m. According to the measurements of the actual surroundings of the Lanzhou-Xinjiang passenger railway of China and mentioned in previous studies (Ma and Ma 2012; Liu 2017; Chen *et al.* 2020), the wind angle between route direction of the railway and prevailing wind direction of strong wind is 75 ~ 105° and accounts for the majority of a whole year's data. Thus, a constant wind of 35 m/s at the three wind angles of 90°, 75°, and 105° was studied based on the high speed and directions of the wind in practice.

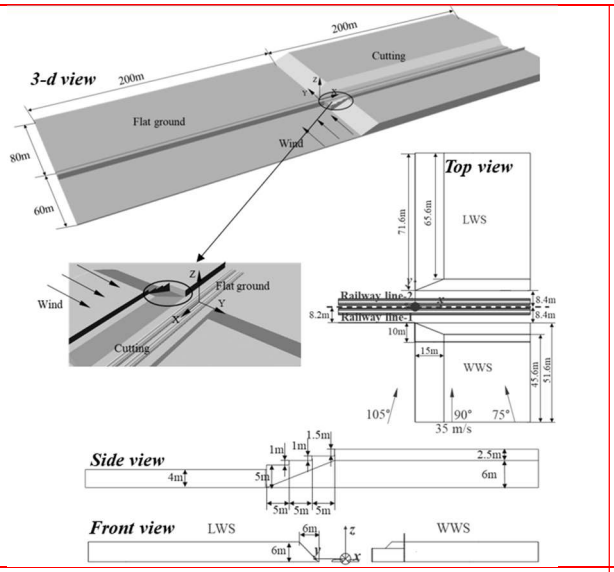

(a) The size of the model

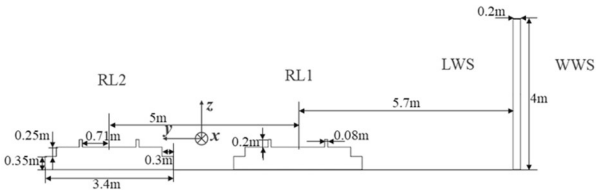

(b) Details of the railway lines

Fig. 13 Computational models

Fig. 14 shows the computational domain and boundary conditions with the wind angle set at 90°. The face BFGC was at the velocity-inlet, and the face AEHD was at the zero pressure-outlet. The ground, windbreak, and railway lines were no-slip walls. The other faces ABCD, DCGH, and EFGH were symmetry conditions. For the case with the wind

angle at 75°, the faces EFGH and BFGC were set as velocity-inlets and the faces ABCD and AEHD were set as zero-pressure outlets. The other boundary conditions remained. For the case with a 105° wind angle, the faces ABCD and BFGC were set as velocity-inlets, the faces EFGH and AEHD were set as zero-pressure outlets, and the other boundary conditions remained the same as that of 90° wind angle. The meshing strategy and the computational method were the same as those of the simulation of the wind tunnel test, so they are not shown again. In addition, the data processing was the same as the previous data processing, but the coordinate system was different from that of the wind tunnel test. The x-axle was along the railway and the y-axle was along the wind direction.

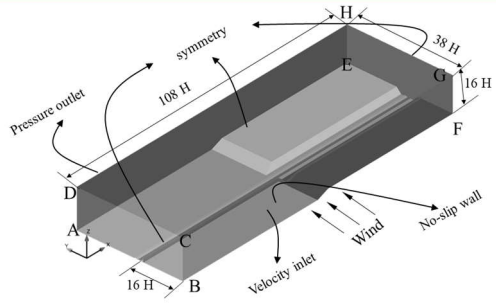

Fig. 14 The computational domain and boundary conditions at the wind angle of 90°

4.2 Velocity distribution of the case with terrain

Horizontal lines parallel to the track at the height of z/H = 0.81 for RL-1 and RL-2 were chosen to analyse the change in the wind velocities around the railway. As shown in Fig. 15, these lines were located on the upper half of the train height range and they could reflect the wind effects on the operation of the train.

Fig. 16 shows the wind velocity along the railway for RL-1 and RL-2. When compared to the flat ground discussed in Section 2, a peak value occurred due to the effect of the terrain. For the case of the wind angle of 90°, and the peak values of u were 0.53 for RL-1 and 0.64 for RL-2. At the wind angle of 75°, the values were 0.42 for RL-1 and 1.03 for RL-2. At the wind angle of 105°, the values were 0.49 for RL-1 and 0.53 for RL-2. It should be noted that due to the effect of the wind angles, the peak values occurred at different locations. Fig. 17 shows the wind velocity distribution from flat ground to cutting for the RL-2 at an angle of 90°. Closer to the flat ground, the shielding effect of the windbreak was good, and the wind velocity was between -0.25–0 in the range of x1–x3. At the windbreak transition region, the wind velocity changed from negative to positive from x4 to x8, and at taller heights, the wind velocity increased, as shown in the circle in Fig. 17(b). At the cutting position, the wind velocity became negative again due to the shielding effect of the cutting height and the windbreak, and the negative wind velocity was larger than that in the position is closer to the flat ground, but as the height increased, the negative values were smaller, indicating that the shielding effect of the cutting was effective. The wind velocity varied from negative to positive peak values and then changed to negative again very quickly, which would be seen in the regions between the flat ground and the cutting (Fig. 16 and Fig. 17). This phenomenon was a possible cause for the yawing motion of the train and it posed a safety issue for the train passing across this region. The reason for strong wind occurrence is further explained in the following sections.

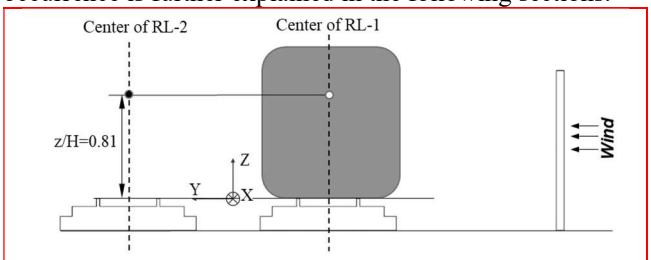

Fig. 15 The analysis position of the wind velocity for the railway

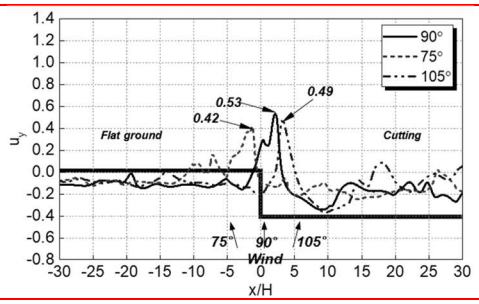

(a) RL-1

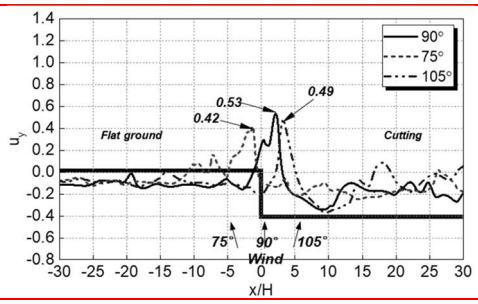

(b) RL-2

Fig. 16 The wind velocity along the railway

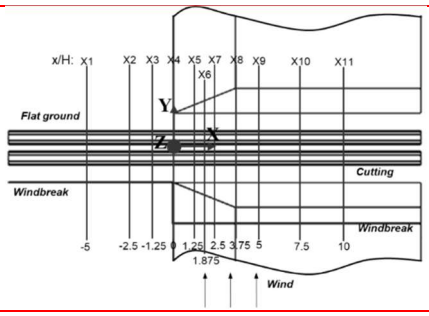

(a) The position of each point

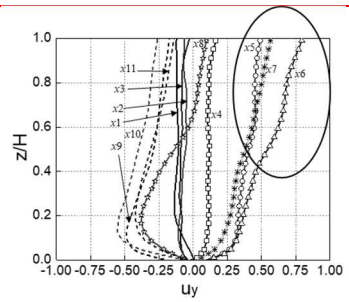

(b) The wind velocity of RL-2

Fig. 17 Wind velocity along the height direction for the case of the wind angle of 90°

4.3 Flow structures of the windbreak transition region

The flow field analysis described in this section was used to explain the reason and mechanism for the sudden changes in wind velocity in the windbreak transition region described in Section 3.2.

4.3.1 Wind angle 90°

At a wind angle of 90°, Fig. 18 shows four vortexes that occurred at the horizon plane, vortexes V1 and V2 that were generated by the stagnation effect of the right-angle area, and vortexes V3 and V4 that were generated inside the windbreak transition area. From z/H = 0.25-1, the structures of V1 and V2 became smaller and they were barely visible at z/H = 1. Inside the windbreak, the core of vortex V3 was always in the position of flat ground and that of V4 was in the cutting area, but as the height increased, the shape of V3 became an asymmetric structure in the region between the railway lines. The effect of V4 on the flow field in the transition region was much stronger. Between vortex V3 and V4, there was a strong wind velocity region, demonstrated by the dashed box in the figure, which was dominated by vortex V4 and which increased as the height increased. Furthermore, Fig. 19 clearly shows the source of vortex V3 and V4. Region A was around the right-angle area of the windbreak structure. The direction and magnitude of the upstream flow changed due to the irregular structure, and the airflow in region A entered the railway as a part of V3 and V4. Region B was in the top of the slope area, and due to the insufficient height of the windbreak, the airflow ran up and rushed into the railway lines directly. Region C was in the top of the cutting and the airflow ran into the cutting and generated the backflow and flows through vortexes V3 and V4. It could also be seen that the strength of V3 and V4 and the sudden wind velocity change in the windbreak transition were mainly influenced by regions A and B.

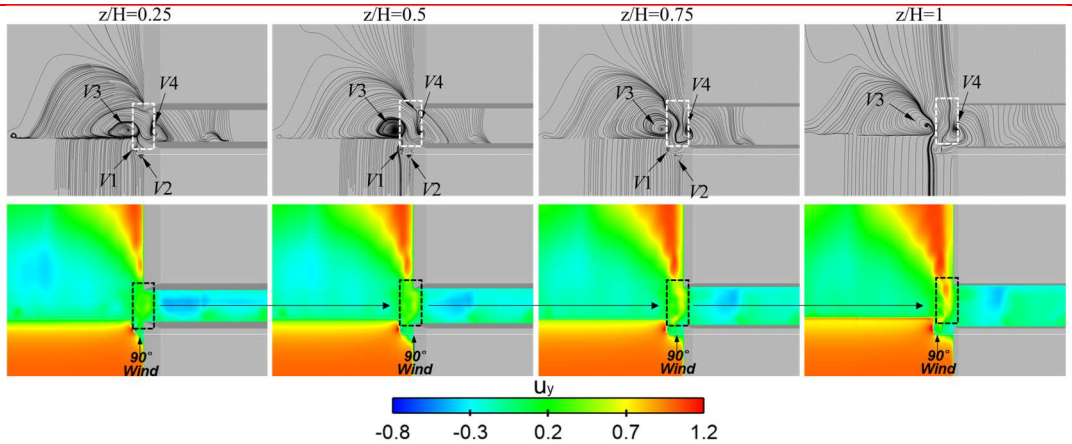

Fig. 18 The streamline and velocity contours at different heights for the wind angle of 90°

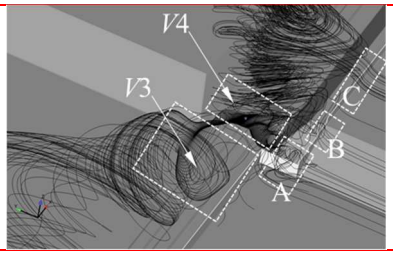

Fig. 19 Three-dimensional streamlines in the region of windbreak transition for the wind angle of 90°

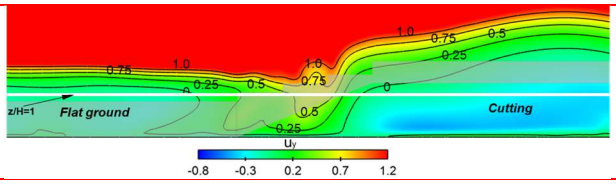

Fig. 20 The velocity contours at the centre between RL-1

and RL-2 for a wind angle of 90°

Finally, to show the impact of the windbreak transition on the wind velocity distribution above the railway intuitively, the velocity contour in the centre between RL-1 and RL-2 is shown in Fig. 20. It can be seen that below the height z/H = 1, the wind velocities in the flat ground and cutting were entirely negative. However, there were positive wind velocity values (larger than 0.5) that occurred between these negative values, as induced by the windbreak transition.

4.3.2 Wind angle 75°

Fig. 21 shows the velocity streamlines and contours at different heights at a wind angle of 75°. Similar to the wind angle of 90°, four vortexes occurred around the windbreak transition region. However, the position of the vortex changed due to the effect of the wind angle. Outside the windbreak, the vortex V1 was generated by the intersection effect between the flat ground and the cutting windbreak. Inside the windbreak, V2 was generated by the windbreak connection part and the corner at the bottom of the slope. Due to the effect of the wind angle, V3 and V4 moved to the flat ground when compared to the wind angle at 90°. As the height increased, V1 remained unchanged. However, V2 changed position from the windbreak connection and moved to the right side at the corner at the bottom of the slope. The vortex core of V3 became smaller and moved to the left flat ground gradually. At the same time, the vortex core of V4 moved to the LWS with the increasing height. Similar to the results of the wind angle at 90°, the wind velocity was larger in a higher position, as shown in the dashed box. In contrast to the wind angle at 90°, the strong wind velocity occurred on the side of the flat ground due to the effect of the wind angle.

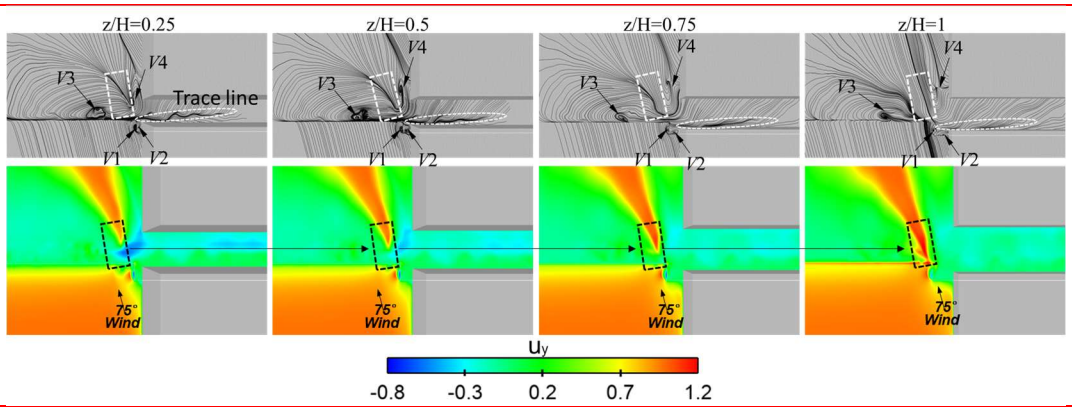

Fig. 21 The streamlines and the velocity contour at different heights for a wind angle of 75°

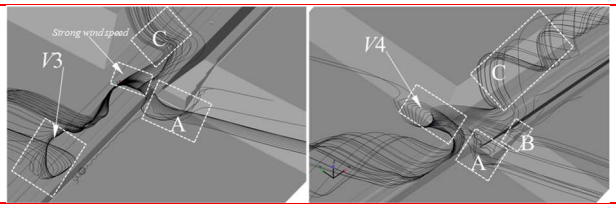

Fig. 22 Three-dimensional streamlines in the region of the windbreak transition for a wind angle of 75°

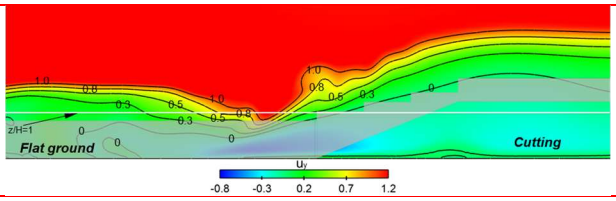

Fig. 23 The velocity contours in the centre between RL-1 and RL-2 for a wind angle of 75°

Furthermore, Fig. 22 shows the space streamlines that contributed to the generation of vortex V3 and vortex V4. Regions A and C were the sources of vortex V3, and regions A, B, and C were the source of vortex V4. Similar to that of wind angle 90°, region C was the airflow that only ran through V3 and V4. The right-angle structure of the windbreak transition (region A) and the insufficient height (region B) were the causes of the sudden positive wind velocity values. This indicated that although the strong wind velocity occurred on the side of the flat ground, it was caused by the windbreak transition region instead of the windbreak in the position of the flat ground. Fig. 23 shows the velocity contour for the velocity distribution between RL-1 and RL-2, and it can be seen that due to the effect of the windbreak transition, a strong positive wind velocity value took place to the left of the transition region closer to the flat ground with a value more than 0.8 below z/H = 1.

4.3.3 Wind angle 105°

Fig. 24 shows the streamlines and speed contours at different heights at a wind angle of 105°. Outside the windbreak, vortex V1 was generated by the bottom of the slope. Inside the windbreak, vortex V2 was generated by the corner of the right-angle structure. Both vortexes were affected by the wind angle. Part of the airflow came from the windbreak transition region, was stopped by the LWS of the cutting wall, and generated vortex V3. The other airflow also came from the windbreak transition region and generated vortex V4 in the cutting outlet location. The results were different from those of the wind angles of 90° and 75°, and V3 and V4 occurred on the side of the cutting due to the effects of the wind angle. Additionally, with the combined

effect of the wind angle and the airflow source, a trace line can be observed in the figure in the dashed circle from V4 to V3. As the height changed from z/H = 0.25 to 1, vortex V1 became invisible. V2 moved from the windbreak connection to the right corner of the bottom slope, which was similar to the movement with the angle of 75°. The position of V3 did not change, but the core was more visible. The core of vortex V4 moved to the left, and it became smaller in size. Meanwhile, as shown in the dashed box, the wind speed became increasingly stronger and positive with an increase in height. Similar to the angles of 90° and 75°, the effect of vortex V4 was the dominant factor for the sudden change in the wind speed. Between the vortexes V4 and V3, there was a negative wind speed area located on the trace line run that decreased with an increase in the height.

For an intuitive view, Fig. 25 shows the space streamline in the region of windbreak transition, and it can be seen that the airflow sources of vortex V3 and V4 came from regions A and B, similar to 90° and 75°. However, the contribution from the cutting decreased due to the wind angle with air entering the region instead of leaving, in turn, this generated vortex V3 and the airflow left the cutting and moved downstream of the domain. Fig. 26 shows the overall speed contour along the centre of the railway between RL-1 and RL-2. It can be seen that due to the impact of the windbreak transition; the sudden change in the speed value was larger than 0.5 in railway lines below the height of z/H = 1.

It could be observed clearly that the right-angle transition of the windbreak had a significant impact on the wind speeds and flow field structures in the railway lines; however, different conditions produced different results. The flat ground outside the windbreak transition consisted of a small effect on the wind speed below the height of z/H = 1 in the railway. This could possibly be explained by the effective height of the windbreak transition in the flat ground did not change. Therefore, the shielding effect did not change significantly around the windbreak transition regions.

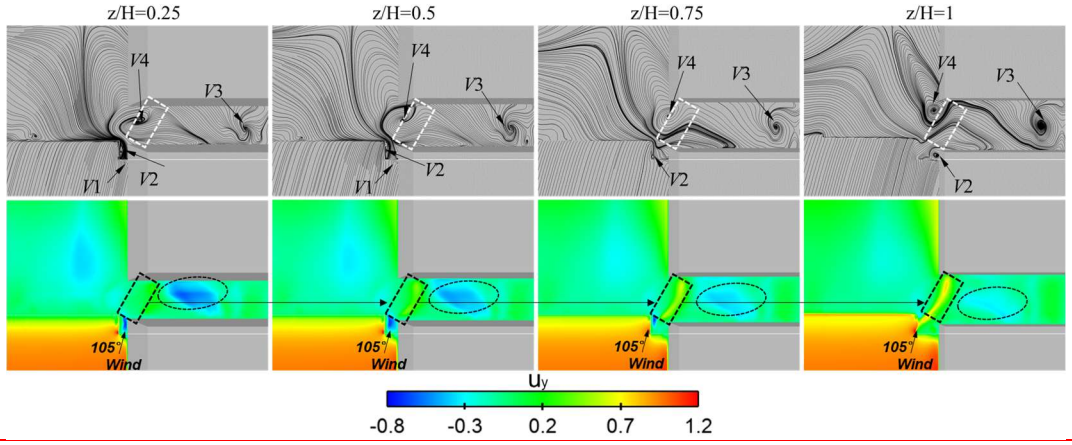

Fig. 24 The streamline and speed contour at different heights for the wind angle of 105°

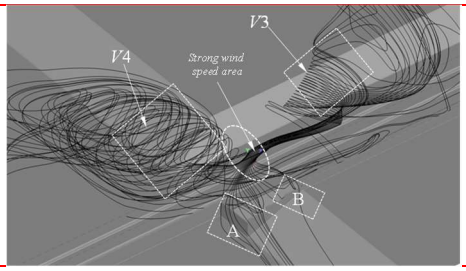

Fig. 25 Three-dimensional streamlines in the region of windbreak transition for the wind angle of 105°

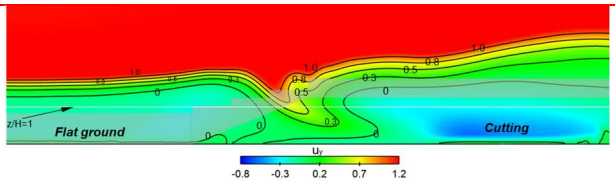

Fig. 26 The speed contour in the centre between RL-1 and RL-2 for the wind angle of 105°

In practice, due to the irregular and continuous terrain, the windbreak had to be built discontinuously and irregularly, such as for the case from flat ground to cutting. These cases depict real situations such as the Lanzhou-Xinjiang railway of China. Based on the results mentioned in Section 3.2–3.3, it could be found that due to the effect of the terrain, the windbreak transition had a large impact on the wind speed distribution and flow structures of the railway lines. Also, the impact of the windbreak transition was different at varying wind angles. In this work, overall, it was found that the impact of a wind angle of 75° was the largest. This is because this wind angle was coincidentally along the slope direction. The impact of the wind angle of 105° was the smallest. This was because the slope and the connection part of the windbreak provided extra resistance to the airflow of the wind angle of 105°.

At different wind angles, the similarity in the results lay in the fact that the effects of the wind speed coeifficent in the railway lines were all larger than 0.5. In addition, the sudden strong wind speed areas of the three wind angles were all induced by the right-angle structures of the windbreak transition region. However, their impact mechanisms were different, which can be seen clearly in the flow field demonstrated in Section 3.3. Predominantly, at a wind angle

of 90°, the airflow sped up directly into the railway lines. This generated a strong and positive wind speed area in the middle of the windbreak transition (x/H = 0–3.75). At a wind angle of 75°, the flow of the air sped up along the slope direction then made its way into the windbreak of the flat ground. This finally generated a vortex in the range of the railway lines. Therefore, a strong and positive wind speed area occurred in the flat ground, but this position of the flat ground was near the beginning of the windbreak transition (x/H = -3–0). At a wind angle of 105°, the flow of air also sped into railway lines, similar to the results achieved at a wind angle of 90°. However, in this case, the strong and positive wind speed area occurred near the end position of the windbreak transition (x/H = 3–5).

5. Conclusions and future work

The results obtained in this work are specific to the modelled flow, and thus they may have some differences with full-scale situations wherein the train windbreaks are embedded in a turbulent shear flow. But consider the height range of the windbreak in practice was not extremely high, and a wind speed in this height range changes only slightly, the research results can still be used as a reference to guide actual research to some extent. Through the analysis and discussion of results, the following conclusions were drawn:

- The wind tunnel tests and the validation of the corresponding numerical simulations indicated that the method in this work was appropriate. Furthermore, the results showed that for the windbreak transition in the case of flat ground had little effect on the train.
- Considering the terrain from the flat ground to cutting, which was closer to the real case, at the height z/H = 0.81 of railway line 1 (RL-1), the sudden peak values of the wind speed coefficient that occurred in the windbreak transition area were 0.53, 0.42, and 0.49 at the wind angles of 90°, 75°, and 105°, respectively. The corresponding wind speed coefficients were 0.64, 1.03, and 0.53, respectively, for railway line 2 (RL-2).
- The space streamlines helped when finding the source of vortexes occurring around the railway lines. Thus, this showed the reasons behind the sudden, strong, and positive wind speed areas. One reason for this was based on the right-angle structure of the windbreak transition, which resulted in sudden wind speed and direction changes. The other reason was based on the insufficient height or the height mismatch in the transition region, which resulted in a decrease in the protective effect of the windbreak.

Based on these results, the flow field deterioration mechanism induced by the windbreak transition was determined and understood. However, future studies could investigate the corresponding mitigation measures to reduce the impact of a windbreak transition.

Acknowledgments

This work was supported by the National Natural Science Foundation of China (Grant No. 52202426, U1334205). the National Key R&D Program of China (Grant No. 2020YFA0710903), the Open Project of Key Laboratory of Traffic Safety on Track of Ministry of Education, Central South University (Grant No. 502401002), the Hong Kong and Macau Joint Research and Development Fund of Wuyi University (Grant No. 2019WGALH15, 2019WGALH17, and 2021WGALH15), and the Natural Science Foundation of Hunan Province, China (Grant No. 2020JJ4737).

References

Baker, C., Cheli, F., Orellano, A., Paradot, N., Proppe, C. and Rocchi, D. (2009), "Cross-wind effects on road and rail vehicles", *Vehicle system dynamics*. **47**(8), 983-1022. https://doi.org/10.1080/00423110903078794

Boldes, U., Colman, J. and Di Leo, J.M. (2001), "Field study of the flow behind single and double row herbaceous windbreaks", *Journal of Wind Engineering and Industrial Aerodynamics*. **89**(7-8), 665-687. https://doi.org/10.1016/S0167-6105(01)00065-4

Boldes, U., Golberg, A., Di Leo, J.M., Colman, J. and Scarabino, A. (2002), "Canopy flow and aspects of the response of plants protected by herbaceous shelterbelts and wood fences", *Journal of Wind Engineering and Industrial Aerodynamics*. **90**(11), 1253-1270. https://doi.org/10.1016/S0167-6105(02)00256-8

Cheli, F., Ripamonti, F., Rocchi, D. and Tomasini, G. (2010), "Aerodynamic behaviour investigation of the new EMUV250 train to cross wind", *Journal of Wind Engineering and Industrial Aerodynamics*. **98**(4-5), 189-201. https://doi.org/10.1016/j.jweia.2009.10.015

Chen, Z.-W., Liu, T.-H., Yan, C.-G., Yu, M., Guo, Z.-J. and Wang, T.-T. (2019), "Numerical simulation and comparison of the slipstreams of trains with different nose lengths under crosswind", *Journal of Wind Engineering and Industrial Aerodynamics*. **190** 256-272. https://doi.org/10.1016/j.jweia.2019.05.005

Chen, Z.-W., Ni, Y.-Q., Wang, Y.-W., Wang, S.-M. and Liu, T.-H. (2022), "Mitigating crosswind effect on high-speed trains by active blowing method: a comparative study", *Engineering Applications of Computational Fluid Mechanics*. **16**(1), 1064-1081. https://doi.org/10.1080/19942060.2022.2064921

Chen, Z., Liu, T., Jiang, Z., Guo, Z. and Zhang, J. (2018), "Comparative analysis of the effect of different nose lengths on train aerodynamic performance under crosswind", *Journal of Fluids and Structures*. **78** 69-85. https://doi.org/10.1016/j.jfluidstructs.2017.12.016

Chen, Z., Liu, T., Li, M., Yu, M., Lu, Z. and Liu, D. (2019), "Dynamic response of railway vehicles under unsteady aerodynamic forces caused by local landforms", *Wind and Structures*. **29**(3), 149-161. https://doi.org/10.12989/was.2019.29.3.149

Chen, Z., Liu, T., Yu, M., Chen, G., Chen, M. and Guo, Z. (2020), "Experimental and numerical research on wind characteristics affected by actual mountain ridges and windbreaks: a case study of the Lanzhou-Xinjiang high-speed railway", *Engineering Applications of Computational Fluid Mechanics*. **14**(1), 1385-1403. https://doi.org/10.1080/19942060.2020.1831963

Chen, Z. and Ni, Y. (2022), "Sudden flow induced by mountain ridges beside windbreaks in a railway and its mitigation measures", *Transportation Safety and Environment*. **4**(1), tdac004. https://doi.org/10.1093/tse/tdac004

Cui, T., Zhang, W. and Sun, B. (2014), "Investigation of train safety domain in cross wind in respect of attitude change", *Journal of Wind Engineering and Industrial Aerodynamics*. **130** 75-87. https://doi.org/10.1016/j.jweia.2014.04.006

Deng, E., Yang, W., Lei, M., Zhu, Z. and Zhang, P. (2019), "Aerodynamic loads and traffic safety of high-speed trains when passing through two windproof facilities under crosswind: A comparative study", *Engineering Structures*. **188** 320-339. https://doi.org/10.1016/j.engstruct.2019.01.080

Diedrichs, B., Sima, M., Orellano, A. and Tengstrand, H. (2007), "Crosswind stability of a high-speed train on a high embankment", *Proceedings of the Institution of Mechanical Engineers, Part F: Journal of Rail and Rapid Transit*. **221**(2), 205-225. https://doi.org/10.1243/0954409JRRT126

Dong, X., Liu, T., Xia, Y., Yang, F., Chen, Z. and Guo, Z. (2022), "Comparative analysis of the aerodynamic performance of trains and dynamic responses of catenaries for windbreak walls with different heights under crosswind", *Proceedings of the Institution of Mechanical Engineers, Part F: Journal of Rail and Rapid Transit*. **0**(0), 1-12. https://doi.org/10.1177/09544097221112506

Flynn, D., Hemida, H., Soper, D. and Baker, C. (2014), "Detached-eddy simulation of the slipstream of an operational freight train", *Journal of Wind Engineering and Industrial Aerodynamics*. **132** 1-12. https://doi.org/10.1016/j.jweia.2014.06.016

Gao, H., Liu, T., Gu, H., Jiang, Z., Huo, X., Xia, Y. and Chen, Z. (2021), "Full-scale tests of unsteady aerodynamic loads and pressure distribution on fast trains in crosswinds", *Measurement*. **186** 110152. https://doi.org/10.1016/j.measurement.2021.110152

Gu, H., Liu, T., Jiang, Z. and Guo, Z. (2020), "Research on the wind-sheltering performance of different forms of corrugated wind barriers on railway bridges", *Journal of Wind Engineering and Industrial Aerodynamics*. **201** 104166. https://doi.org/10.1016/j.jweia.2020.104166

Guo, Z., Liu, T., Chen, Z., Xia, Y., Li, W. and Li, L. (2020), "Aerodynamic influences of bogie's geometric complexity on high-speed trains under crosswind", *Journal of Wind Engineering and Industrial Aerodynamics*. **196** 104053. https://doi.org/10.1016/j.jweia.2019.104053

Hashmi, S.A., Hemida, H. and Soper, D. (2019), "Wind tunnel testing on a train model subjected to crosswinds with different windbreak walls", *Journal of Wind Engineering and Industrial Aerodynamics*. **195** 104013. https://doi.org/10.1016/j.jweia.2019.104013

He, X., Zhou, L., Chen, Z., Jing, H., Zou, Y. and Wu, T. (2019), "Effect of wind barriers on the flow field and aerodynamic forces of a train–bridge system", *Proceedings of the Institution of Mechanical Engineers, Part F: Journal of Rail and Rapid Transit*. **233**(3), 283-297. https://doi.org/10.1177/0954409718793220

Hemida, H. and Krajnović, S. (2008), "LES study of the influence of a train-nose shape on the flow structures under cross-wind conditions", *Journal of Fluids Engineering*. **130**(9), 091101. https://doi.org/10.1115/1.2953228

Huo, X., Liu, T., Yu, M., Chen, Z., Guo, Z., Li, W. and Wang, T. (2021), "Impact of the trailing edge shape of a downstream dummy vehicle on train aerodynamics subjected to crosswind", *Proceedings of the Institution of Mechanical Engineers, Part F: Journal of Rail and Rapid Transit*. **235**(2), 201-214. https://doi.org/10.1177/0954409720915039

Krajnovic, S. (2008). "Numerical simulation of the flow around an ICE2 train under the influence of a wind gust". *2008 International Conference on Railway Engineering-Challenges for Railway Transportation in Information Age*, Hong Kong, March. https://ieeexplore.ieee.org/abstract/document/4730862

Krajnović, S., Ringqvist, P., Nakade, K. and Basara, B. (2012), "Large eddy simulation of the flow around a simplified train moving through a crosswind flow", *Journal of Wind Engineering and Industrial Aerodynamics*. **110** 86-99. https://doi.org/10.1016/j.jweia.2012.07.001

Li, W., Liu, T., Martinez-Vazquez, P., Guo, Z., Huo, X., Xia, Y. and Chen, Z. (2022), "Effects of embankment layouts on train aerodynamics in a wind tunnel configuration", *Journal of Wind Engineering and Industrial Aerodynamics*. **220** 104830. https://doi.org/10.1016/j.jweia.2021.104830

Li, Y., Hu, P., Cai, C., Zhang, M. and Qiang, S. (2013), "Wind tunnel study of a sudden change of train wind loads due to the wind shielding effects of bridge towers and passing trains", *Journal of Engineering Mechanics*. **139**(9), 1249-1259. https://doi.org/10.1061/(ASCE)EM.1943-7889.0000559

Li, Y., Zhang, J., Zhang, M., Wang, Z. and Guo, J. (2019), "Aerodynamic effects of viaduct-cutting connection section on high-speed railway by wind tunnel tests", *Journal of Aerospace Engineering*. **32**(5), 05019002. https://doi.org/10.1061/(ASCE)AS.1943-5525.0001065

Liu, B. (2017), "Wind Characteristic Analysis of 100-Kilometer Wind Area in Lanzhou-Xinjiang High-Speed Railway", *2nd International Conference on Industrial Aerodynamics (ICIA 2017)*. 562-571. https://scholar.google.com.hk/scholar?hl=zh-CN&as_sdt=0%2C5&q=Wind+Characteristic+Analysis+of+100-Kilometer+Wind+Area+in+Lanzhou-Xinjiang+High-Speed+Railway&btnG=

Liu, T.-H., Wang, L., Chen, Z.-W., Gao, H.-R., Li, W.-H., Guo, Z.-j., Xia, Y.-T., Huo, X.-S. and Wang, Y.-W. (2022), "Study on the pressure pipe length in train aerodynamic tests and its applications in crosswinds", *Journal of Wind Engineering and Industrial Aerodynamics*. **220** 104880. https://doi.org/10.1016/j.jweia.2021.104880

Liu, T., Chen, Z., Zhou, X. and Zhang, J. (2018), "A CFD analysis of the aerodynamics of a high-speed train passing through a windbreak transition under crosswind", *Engineering Applications of Computational Fluid Mechanics*. **12**(1), 137-151. https://doi.org/10.1080/19942060.2017.1360211

Ma, S. and Ma, Y. (2012). "Study on preventing and controlling strong wind disaster on high-speed railway". *Proceedings of the 1st International Workshop on High-Speed and Intercity Railways*. https://doi.org/10.1007/978-3-642-27960-7

Mohebbi, M. and Rezvani, M.A. (2018), "Two-dimensional analysis of the influence of windbreaks on airflow over a high-speed train under crosswind using lattice Boltzmann method", *Proceedings of the Institution of Mechanical Engineers, Part F: Journal of Rail and Rapid Transit*. **232**(3), 863-872. https://doi.org/10.1177/0954409717699502

Mohebbi, M. and Rezvani, M.A. (2019), "Analysis of the effects of lateral wind on a high speed train on a double routed railway track with porous shelters", *Journal of Wind Engineering and Industrial Aerodynamics*. **184** 116-127. https://doi.org/10.1016/j.jweia.2018.11.011

Mohebbi, M. and Rezvani, M.A. (2021), "2D and 3D numerical and experimental analyses of the aerodynamic effects of air fences on a high-speed train", *Wind and Structures*. **32**(6), 539-550. https://doi.org/10.12989/was.2021.32.6.539

Mohebbi, M. and Safaee, A.M. (2021), "The optimum model determination of porous barriers in high-speed tracks", *Proceedings of the Institution of Mechanical Engineers, Part F: Journal of Rail and Rapid Transit*. 0954409721995323. https://doi.org/10.1177/0954409721995323

Niu, J., Wang, Y., Liu, F. and Chen, Z. (2020), "Comparative study on the effect of aerodynamic braking plates mounted at the inter-carriage region of a high-speed train with pantograph and air-conditioning unit for enhanced braking", *Journal of Wind Engineering and Industrial Aerodynamics*. **206** 104360. https://doi.org/10.1016/j.jweia.2020.104360

Niu, J., Zhang, Y., Li, R., Chen, Z., Yao, H. and Wang, Y. (2022), "Aerodynamic simulation of effects of one-and two-side windbreak walls on a moving train running on a double track railway line subjected to strong crosswind", *Journal of Wind Engineering and Industrial Aerodynamics*. **221** 104912. https://doi.org/10.1016/j.jweia.2022.104912

Niu, J., Zhou, D. and Wang, Y. (2018), "Numerical comparison of

aerodynamic performance of stationary and moving trains with or without windbreak wall under crosswind", *Journal of Wind Engineering and Industrial Aerodynamics*. **182** 1-15. https://doi.org/10.1016/j.jweia.2018.09.011

Pieris, S., Tuna, B., Yarusevych, S. and Peterson, S. (2020), "Flow development upstream of a fence", *International Journal of Heat and Fluid Flow*. **82** 108565. https://doi.org/10.1016/j.ijheatfluidflow.2020.108565

Shur, M.L., Spalart, P.R., Strelets, M.K. and Travin, A.K. (2008), "A hybrid RANS-LES approach with delayed-DES and wall-modelled LES capabilities", *International journal of heat and fluid flow*. **29**(6), 1638-1649. https://doi.org/10.1016/j.ijheatfluidflow.2008.07.001

Spalart, P.R., Deck, S., Shur, M.L., Squires, K.D., Strelets, M.K. and Travin, A. (2006), "A new version of detached-eddy simulation, resistant to ambiguous grid densities", *Theoretical and computational fluid dynamics*. **20**(3), 181-195. https://doi.org/10.1007/s00162-006-0015-0

Sui, Y., Niu, J., Ricco, P., Yuan, Y., Yu, Q., Cao, X. and Yang, X. (2021), "Impact of vacuum degree on the aerodynamics of a high-speed train capsule running in a tube", *International Journal of Heat and Fluid Flow*. **88** 108752. https://doi.org/10.1016/j.ijheatfluidflow.2020.108752

Sun, Z., Hashmi, S.A., Dai, H., Cheng, X., Zhang, T. and Chen, Z. (2021), "Safety comparisons of a high-speed train's head and tail passing by a windbreak breach", *Vehicle system dynamics*. **59**(6), 823-840. https://doi.org/10.1080/00423114.2020.1725067

Tan, C., Zhou, D., Chen, G., Sheridan, J. and Krajnovic, S. (2020), "Influences of marshalling length on the flow structure of a maglev train", *International Journal of Heat and Fluid Flow*. **85** 108604. https://doi.org/10.1016/j.ijheatfluidflow.2020.108604

TFI (2015), *Turbulent Flow instrumentation - cobra probe - getting Started Guide*, Turbulent Flow Instrumentation Pty Ltd.https://www.turbulentflow.com.au/Downloads/Getting%20Started%20-%20Cobra%20Probe.pdf

Tian, H. (2010), "Research progress in railway safety under strong wind condition in China", *Journal of Central South University (Science and Technology)*. **41**(6), 2435-2443. https://doi.org/CNKI:SUN:ZNGD.0.2010-06-063

Tian, H. (2019), "Review of research on high-speed railway aerodynamics in China", *Transportation Safety and Environment*. **1**(1), 1-21. https://doi.org/10.1093/tse/tdz014

Tsubokura, M., Nakashima, T., Kitayama, M., Ikawa, Y., Doh, D.H. and Kobayashi, T. (2010), "Large eddy simulation on the unsteady aerodynamic response of a road vehicle in transient crosswinds", *International Journal of Heat and Fluid Flow*. **31**(6), 1075-1086. https://doi.org/10.1016/j.ijheatfluidflow.2010.05.008

Tunay, T., Firat, E. and Sahin, B. (2018), "Experimental investigation of the flow around a simplified ground vehicle under effects of the steady crosswind", *International Journal of Heat and Fluid Flow*. **71** 137-152. https://doi.org/10.1016/j.ijheatfluidflow.2018.03.020

Van Doormaal, J.P. and Raithby, G.D. (1984), "Enhancements of the SIMPLE method for predicting incompressible fluid flows", *Numerical heat transfer*. **7**(2), 147-163. https://doi.org/10.1080/01495728408961817

Wang, J., Minelli, G., Dong, T., Chen, G. and Krajnović, S. (2019), "The effect of bogie fairings on the slipstream and wake flow of a high-speed train. An IDDES study", *Journal of Wind Engineering and Industrial Aerodynamics*. **191** 183-202. https://doi.org/10.1016/j.jweia.2019.06.010

Xu, J., Chen, Z. and Liu, T. (2019). "Experimental and numerical research on the safety of an EMU running on a normal-speed railway line under strong wind". *Conference: 2019 3th International Conference on Traffic Engineering and Transportation System (ICTETS 2019)*, Jiaozuo. https://doi.org/10.1088/1757-899X/688/4/044049

Yang, W., Deng, E., Lei, M., Zhu, Z. and Zhang, P. (2019), "Transient aerodynamic performance of high-speed trains when passing through two windproof facilities under crosswinds: A comparative study", *Engineering Structures*. **188** 729-744. https://doi.org/10.1016/j.engstruct.2019.03.070

Yu, H., Wang, B., Li, Y. and Zhang, M. (2019), "Driving risk of road vehicle shielded by bridge tower under strong crosswind", *Natural Hazards*. **96**(1), 497-519. https://doi.org/10.1007/s11069-018-3554-y

Zhang, J., Zhang, M., Li, Y. and Fang, C. (2019), "Aerodynamic effects of subgrade-tunnel transition on high-speed railway by wind tunnel tests", *Wind and Structures*. **28**(4), 203-213. https://doi.org/10.12989/was.2019.28.4.203